ACSNANO

www.acsnano.org

ARTICLE

# AFM Manipulation of EGaIn Microdroplets to Generate Controlled, On-Demand Contacts on Molecular Self-Assembled Monolayers

Eugene Jia Hao Soh, Hippolyte P. A. G. Astier, Dan Daniel,* Jia Qing Isaiah Chua, Ali Miserez, Zian Jia, Ling Li, Sean J. O'Shea,* Harish Bhaskaran,* Nikodem Tomczak,* and Christian A. Nijhuis*

Cite This: *ACS Nano* 2022, 16, 14370–14378

Read Online

ACCESS | Metrics & More | Article Recommendations | Supporting Information

**ABSTRACT:** **Liquid metal droplets, such as eutectic gallium–indium (EGaIn), are important in many research areas, such as soft electronics, catalysis, and energy storage. Droplet contact on solid surfaces is typically achieved without control over the applied force and without optimizing the wetting properties in different environments (e.g., in air or liquid), resulting in poorly defined contact areas. In this work, we demonstrate the direct manipulation of EGaIn microdroplets using an atomic force microscope (AFM) to generate repeated, on-demand making and breaking of contact on self-assembled monolayers (SAMs) of alkanethiols. The nanoscale positional control and feedback loop in an AFM allow us to control the contact force at the nanonewton level and, consequently, tune the droplet contact areas at the micrometer length scale in both air and ethanol. When submerged in ethanol, the droplets are highly nonwetting, resulting in hysteresis-free contact forces and minimal adhesion; as a result, we are able to create reproducible geometric contact areas of 0.8–4.5 $\mu m^2$ with the alkanethiolate SAMs in ethanol. In contrast, there is a larger hysteresis in the contact forces and larger adhesion for the same EGaIn droplet in air, which reduced the control over the contact area (4–12 $\mu m^2$). We demonstrate the usefulness of the technique and of the gained insights in EGaIn contact mechanics by making well-defined molecular tunneling junctions based on alkanethiolate SAMs with small geometric contact areas of between 4 and 12 $\mu m^2$ in air, 1 to 2 orders of magnitude smaller than previously achieved.**

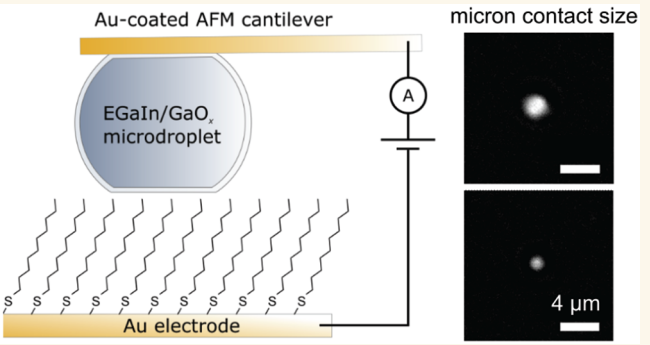


**KEYWORDS:** *atomic force microscopy, micromanipulation, EGaIn, liquid metal, molecular electronics*

## INTRODUCTION

Eutectic gallium–indium metal alloy (EGaIn) is a nontoxic liquid at room temperature with a unique combination of rheological, thermal, and electrical properties that makes it attractive for applications in soft electronics,[1−3] catalysis,[4] energy storage,[5,6] plasmonics,[7,8] 2D-materials synthesis,[9] and molecular electronics.[10−13] In the presence of oxygen, a self-passivating 0.7–2 nm thick gallium oxide layer forms spontaneously at the exposed interface, endowing EGaIn with non-Newtonian rheological properties;[14,15] as a result, liquid EGaIn can be molded into various geometries (e.g., micro/nano-sized spheres,[15,16] rods,[17] and cones,[10] or injected into microchannels[11]).

To incorporate EGaIn into devices, different methods have been developed to spatially manipulate and position EGaIn (e.g., using magnetic fields,[18−20] microfluidics, and conventional patterning/fabrication techniques[11,21,22]). However, these techniques lack the precise nanometric positioning to control the applied forces and, hence, tune the contact areas on different surfaces (e.g., molecular monolayers, organic thin films, or elastomers) and in different ambient environments (e.g., in air and liquids). There is also little understanding of how the ambient environment affects the surface wetting properties and the contact mechanics of EGaIn. Moreover, the forces typically applied to EGaIn when using conventional fabrication methods are large enough to induce cracks and

Received: May 12, 2022
Accepted: August 30, 2022
Published: September 6, 2022

wrinkles on the oxide surface, possibly reducing surface adhesion and leading to smaller effective contact areas.

In this paper, we manipulate EGaIn microdroplets using an atomic force microscope (AFM) to achieve controlled, on-demand, micrometer-sized contacts on gold surfaces functionalized with self-assembled monolayers (SAMs) of different *n*-alkanethiolates $S(CH_2)_{n-1}CH_3$, where $n$ = 4, 6, 8, and 10 is the number of carbon atoms (labeled C*n* hereafter). We first fabricated microdroplets of EGaIn using ultrasonication, which we then picked up with a tipless AFM cantilever. The piezomotors of the AFM allowed us to position the attached microdroplet in 3D space with nanometric resolution and to make and break contacts repeatedly at different locations on the surface at will, i.e., forming on-demand contacts. The nanometric positional control and the force feedback loop allow us to control the force applied to the EGaIn droplet with nanonewton resolution and, consequently, tune the contact area with micrometer-scale resolution. The formation of wrinkles and cracks typically observed in EGaIn when contacting a surface at higher applied forces is effectively avoided because of the small forces applied (typically around 10 nN);[23,24] the microdroplets remain spherical and smooth down to the nanoscale even after making repeated contacts. This is important in applications where good conformal (electrical) contact with the target surface is desired, such as in molecular/organic electronics and epidermal electronic devices.

We also found that the wetting behavior and hence the contact mechanics of EGaIn are highly dependent on the ambient environment (e.g., air vs liquid environment), which are reflected in the AFM force spectroscopy measurements.[25−27] In air, an EGaIn droplet makes a contact angle of about 150° on the SAM surface (C4, C6, C8, C10), and there is significant droplet adhesion and hysteresis between the approach and retract force curves. In contrast, when submerged in ethanol, the EGaIn droplet becomes highly nonwetting, forming a contact angle of nearly 180°, with no adhesion and negligible hysteresis in the force spectroscopy curves. A hysteresis-free force curve means that the EGaIn contact area in ethanol only depends on the magnitude of the applied force (i.e., conservative) and not on how the applied force is achieved (i.e., path and rate independent); in contrast, the contact area in air can take on different values for the same magnitude of the applied force (i.e., nonconservative).

We demonstrate the versatility of our approach by making molecular tunneling junctions that incorporate SAMs. There is much interest in using EGaIn as a top electrode in SAM-based molecular electronics because it is easy to implement and results in high yields of devices.[10,28,29] To achieve different electronic properties with SAM, it is important to control the SAM−EGaIn interface with great precision. Yet, when using commonly accepted techniques such as the cone-shaped tip method, the resulting contact area is ill-defined (the effective electrical contact area is $10^4$−$10^6$ times smaller than the geometrical contact area).[24,30−32] In contrast, our technique allows us to make tunneling junctions with defined contact areas of between 4 and 12 $\mu m^2$ in air, 1 to 2 orders of magnitude smaller than previous methods.

To demonstrate that we were forming tunneling junctions and not ohmic contacts, we measured the current density across SAMs (C4, C6, C8, C10) and showed that the tunneling behavior across these junctions is dominated by the molecular structure, with the measured tunneling decay coefficient $\beta = 1.01 \pm 0.04\ n^{-1}$ in line with literature values.[33−35] The junctions formed this way are robust and can withstand voltages of up to 5 V, corresponding to an electric breakdown field of approximately 50 MV $cm^{-1}$, compared to a typical breakdown field of ∼8 MV $cm^{-1}$ in junctions with the same Au/SAM/EGaIn structure formed using the EGaIn cone-shaped tip method.[36] Beyond molecular electronics, the manipulation of EGaIn using AFM has other potential applications, such as in nanowelding,[37] nanoelectronics,[11] and electrical AFM mapping of thin films,[38] where precise positional control of micro/nano-scale liquid metal structures is required.

## RESULTS AND DISCUSSION

**Formation of EGaIn Microdroplet Probes.** EGaIn microdroplets were prepared via ultrasonication in ethanol (20% of EGaIn by weight) for 30 min. The oscillating shear forces during ultrasonication generate polydisperse droplets that range from submicron to tens of microns in diameters. A nanometric oxide layer is quickly formed on the surface of the newly generated droplets, preventing coalescence into larger droplets.[39] Using ethanol as the dispersant medium results in better stability of the EGaIn suspension over time compared to water, likely due to a carbon layer that can act as a surfactant.[1] A small volume (typically 10 $\mu$L) of the EGaIn−ethanol mixture was drop-casted on the SAM surface of interest, and once the ethanol had evaporated, we were able to pick up the EGaIn microdroplet using a tipless AFM cantilever with gold coating on both sides and a spring constant $k$ = 0.5−5 N $m^{-1}$. After choosing a droplet of the desired size as observed under an optical microscope, we approach the microdroplet at a controlled speed of $U = 1\ \mu m\ s^{-1}$ until the cantilever reaches a force set point of about 5 nN, which is sufficient to pick up the EGaIn droplet without plastically deforming it. We then apply a lateral shearing of the cantilever (with a displacement of about 5 $\mu$m) while in contact with the microdroplet to dislodge the droplet from the substrate. At this point, the droplet is attached to the cantilever and remains so even after we retract the cantilever from the surface (Figure 1a).

The resulting droplet is spherical and smooth, despite the shearing. This is evident from the scanning electron micrograph (SEM) in Figure 1b. Moreover, by using tapping mode AFM, we mapped the topography of an EGaIn droplet of radius $R = 1.7\ \mu m$ attached to the AFM cantilever (Figure 1c), with the dots and solid line in Figure 1d showing the radially averaged line section of the same droplet. The resulting topography map is not a sphere because of the tip−sample convolution effect when the sidewall of the tip touches the droplet.[40] We can however fit a circle to the line section to obtain the actual droplet geometry (assumed to be spherical, dashed line in Figure 1d). The fitted geometry has a contact angle $\theta_c = 148°$ on the gold-coated cantilever. By looking at the magnified portion at the droplet peak, we found that the EGaIn droplet is smooth down to the nanoscale, with root-mean-square roughness $\Delta h$ = 1 nm (Figure 1e and Supporting Figure S1). This suggests that our picking up procedure does not deform the microdroplets.

Once picked up, the microdroplet is attached sufficiently strongly to the cantilever to allow us to move the droplet to desired regions on the substrate and form well-defined contacts repeatedly without the droplet detaching. This relatively strong adhesion is induced by the interaction between the surface oxide layer of EGaIn and the gold coating of the cantilever. At



https://doi.org/10.1021/acsnano.2c04667
ACS Nano 2022, 16, 14370−14378

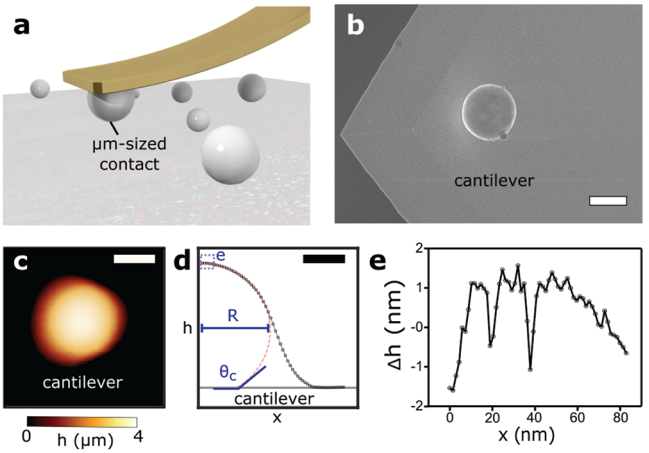


**Figure 1. (a) Manipulation of EGaIn droplets using a tipless AFM cantilever to form micron-sized contacts. (b) SEM image of an EGaIn droplet on an AFM cantilever. Scale bar is 1 $\mu$m. (c) AFM topographic map of the EGaIn droplet on the cantilever. Scale bar is 2 $\mu$m. (d) Radially averaged line section of the topographic image in (c) (experimental data represented by dots and solid line). Scale bar is 1 $\mu$m. Red dashed line represents the best-fit curve when fitting the experimental data with a circle. (e) Line section (not radially averaged) of a magnified region at the peak of the droplet (marked e in d) showing a root-mean-square surface roughness $\Delta h$ = 1 nm.**

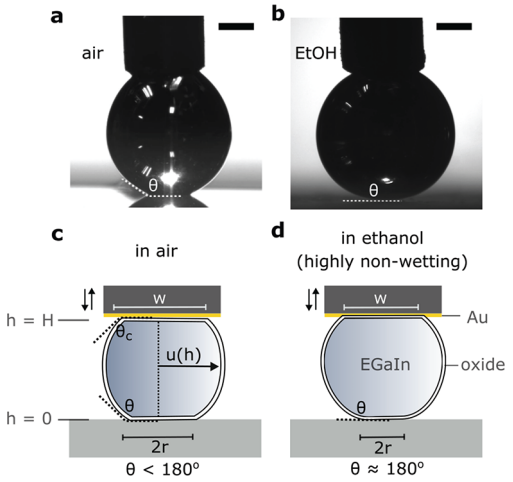


**Figure 2. On the C4 surface, EGaIn droplets make a contact angle of (a) $\theta$ = 148 ± 2° in air and (b) $\theta \approx 180°$ in ethanol. Scale bars are 1 mm in (a) and (b). Droplet geometries in (c) air and (d) ethanol during force spectroscopy measurements.**

the same time, the oxide layer also prevents direct contact of the bulk liquid metal with gold; in the absence of this oxide layer (for example after exposure to hydrochloric acid vapor), EGaIn will alloy with the gold and the droplet will no longer be spherical (Supporting Figure S2). However, we do not rule out the formation of nanocracks in the oxide layer, which allows the EGaIn droplet to form a direct contact with the gold cantilever, contributing to the strong adhesion.

**Contact Mechanics of EGaIn Droplets.** We investigated the contact mechanics of EGaIn droplets on template-stripped gold surfaces functionalized with SAMs (i.e., C4, C6, C8, C10). Alkyl functional groups were chosen because they are known to form stable molecular tunneling junctions,[10,30] and the resulting SAM surfaces are smooth with a root-mean-square surface roughness $\Delta h$ < 1 nm.[41]

The contact angle $\theta$ that a droplet makes on the surface depends on the surface energies of the various interfaces, i.e., the Young's relation:

$$\cos\theta = \frac{\gamma_S - \gamma_{LS}}{\gamma_L} \approx \frac{\gamma_S - 2\sqrt{\gamma_L\gamma_S}}{\gamma_L} \quad (1)$$

where $\gamma_S$ is the solid interfacial energy, $\gamma_L$ is the liquid droplet's interfacial energy, and $\gamma_{LS} \approx 2\sqrt{\gamma_L\gamma_S}$ is the liquid−solid interfacial energy.[42] For a millimetric-sized EGaIn droplet sitting on a C4 surface in air, the balance of the three interfacial energies results in a contact angle $\theta_{exp}$ = 148 ± 2° as measured optically in Figure 2a. The wetting properties of the droplet can be tuned by changing the ambient environment. For example, when we submerge the C4 surface (and other alkyl lengths) in ethanol (or other organic solvent), $\gamma_L \approx \gamma_S$ and $\cos\theta \approx -1$ (see eq 1); the droplet becomes highly nonwetting with $\theta_{exp}$ = 175 ± 5° (Figure 2b).

Detailed contact mechanics of EGaIn microdroplets can be investigated by performing AFM force spectroscopy measurements on the alkanethiol surface C4 in air and in ethanol (Figure 3a,b). The droplet geometries during contact are summarized in Figure 2c,d. Here, after picking up an EGaIn droplet ($R$ = 5 $\mu$m) using a tipless AFM cantilever, we use the piezomotor of the AFM to control the vertical motion of the EGaIn droplet at a speed $U$ = 0.5 $\mu$m s$^{-1}$; at the same time, we can deduce the force $F$ experienced by the droplet from the cantilever deflection. The entire AFM setup is mounted on top of an inverted optical microscope, which allows us to visualize the contact size of the EGaIn droplet using reflection light microscopy. Details of the AFM technique have been described in our previous work and by other groups.[43−46]

Far from the surface, the droplet experiences no force ($F$ = 0), but when the droplet contacts the C4 surface in air (Figure 3a), we observe a sudden capillary snap-in force $F_{snap}$ = 1.6 ± 0.1 $\mu$N due to the surface tension of EGaIn. Since the surface tension of the EGaIn droplet is much larger than that of water, the formation of water capillary bridges due to water capillary condensation is not an important contributing factor to $F_{snap}$[47] (see also discussion on the effect of humidity in Supporting Figure S3). Because the droplet makes a finite contact angle $\theta$ < 180° on the surface, there is strong adhesion to the surface and a critical adhesion force $F_{adh}$ = 2.2 ± 0.1 $\mu$N is required to remove the droplet. We also observed a large hysteresis between the approach and retract curves, represented by the dashed and full lines, respectively, in Figure 3a,b. We can quantify the amount of hysteresis by integrating the area between the approach and retract curves (shaded gray in Figure 3a). The magnitude of the energy loss during one force spectroscopy cycle in air is calculated to be 2.78 ± 0.01 pJ (Figure 3a). In contrast, there is no detectable $F_{snap}$ for an EGaIn droplet of similar size ($R$ = 6 $\mu$m) contacting the same C4 surface in ethanol; the adhesion is minimal with $F_{adh}$ = 1 nN, and there is little hysteresis between the approach and retract curves with an energy loss calculated to be 1.0 ± 0.1 fJ (Figure 3b). The small discrete force jumps of magnitudes $\delta F$ = 1−3 nN in the approach and retract curves are likely due to the stick−slip motion of the contact line; this indicates that the droplets in ethanol are slightly pinned.

The force experienced by the microdroplet $F$ is related to the contact radius $r$ and contact angle $\theta$, since


https://doi.org/10.1021/acsnano.2c04667
ACS Nano 2022, 16, 14370−14378

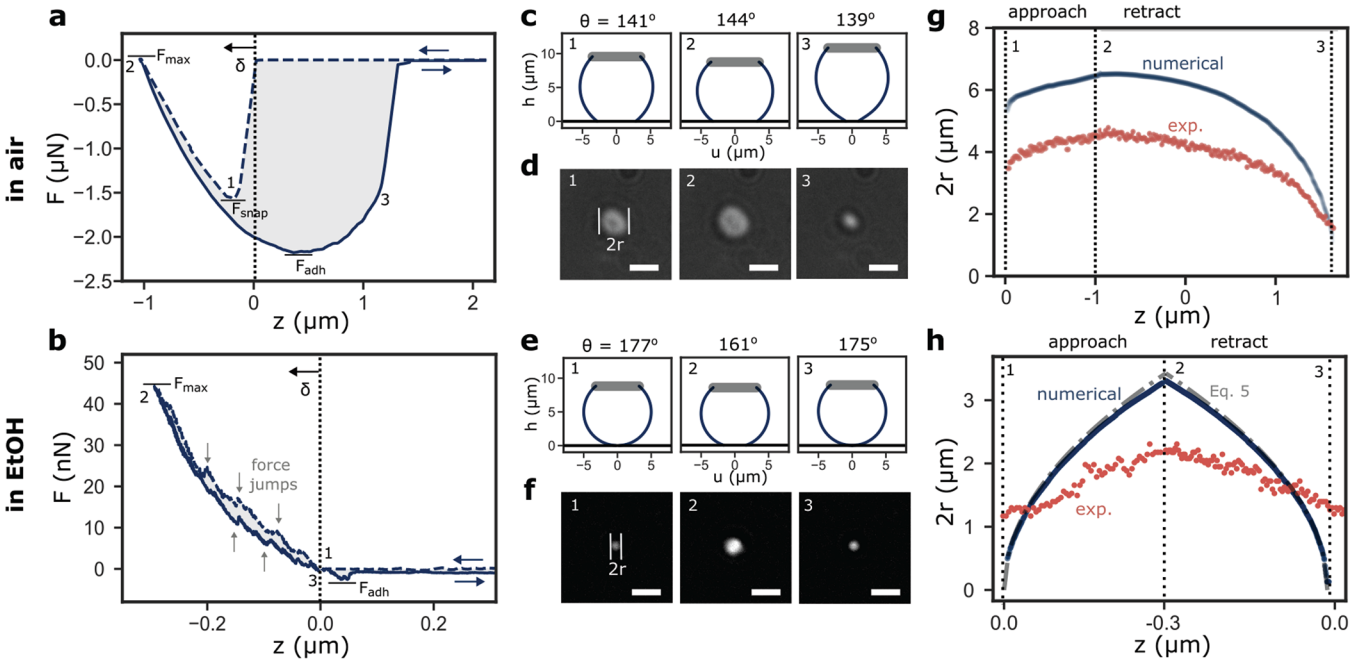


**Figure 3. (a, b) Force spectroscopy of an EGaIn droplet ($R$ = 5, 6 $\mu$m) contacting the C4 surface in air and in ethanol, respectively. $z$ is the droplet position after correcting for cantilever deflection. Large positive values of $z$ correspond to the tip being far from the surface, and $z$ = 0 is defined as the position where the tip contacts the surface on approach. The indentation depth $\delta$, equivalent to $z$, can be defined when the tip is in contact with the surface. (c) Droplet geometries in air are obtained by solving the Young−Laplace equation, (d) while the contact area is visualized using reflection light microscopy. Scale bars are 4 $\mu$m. (e, f) The corresponding droplet geometries and micrographs in ethanol. Scale bars are 4 $\mu$m. (g, h) Comparison between the droplet contact diameter 2$r$ as predicted by the Young−Laplace equation (blue lines) and observed experimentally by microscopy (red dots) in air and in ethanol, respectively.**

$$F = -2\pi\gamma r \sin\theta + \pi r^2 \Delta P \tag{2}$$

where $\Delta P \approx 2\gamma/R$ is the Laplace pressure inside the droplet of radius $R$, and $\gamma$ = 620 mN m$^{-1}$ is the surface tension determined using the pendant-drop method (Supporting Figure S4)[48] and is consistent with previously reported values.[11,49] At the same time, the droplet shape $u(h)$ is described by the axisymmetric Young−Laplace equation

$$\begin{aligned} &\frac{u''}{(1+u'^2)^{3/2}} - \frac{1}{u\sqrt{1+u'^2}} = -\Delta P/\gamma \\ &u(H) = w/2 \\ &u(0) = r \\ &\int_0^H \pi u^2 \mathrm{d}h = v \end{aligned} \tag{3}$$

where $w$ is the droplet contact size on the cantilever and $H$ and $v$ are the droplet's height and volume, respectively (see geometry in Figure 2c,d). Here, we assume that the contact mechanics and the force experienced by the droplet are dominated by the surface tension of EGaIn and not by the mechanical properties of the oxide skin (Young's modulus $E \sim$ 1 GPa[50,51]). A justification for this approach can be found in Supporting Figure S5. By solving eqs 2 and 3 numerically, we can deduce the droplet's geometry both in air and in ethanol (Figure 3c,e), from the point of contact (position 1), to the maximal loading force (position 2), and just before detaching from the surface (position 3). The numerical scheme used to solve the Young−Laplace equation has been described in our previous work[52] and summarized in Supporting Figure S5. The numerical results for $r_{num}$ can then be compared with $r_{exp}$ values experimentally determined by reflection light microscopy (Figure 3d,f). See Supporting Videos S1−S4 for the full numerical and microscopy results.

We observed that the range of force-dependent contact angles obtained numerically for the EGaIn microdroplets $\theta_{num}$ = 139−144° in air (Figure 3c) and $\theta_{num}$ = 161−177° in ethanol (Figure 3e) are in agreement with those measured optically for millimetric-sized droplets (Figure 2a,b). EGaIn is highly nonwetting when submerged in ethanol, and this explains why $r$ is consistently smaller in ethanol (Figure 3f) than in air (Figure 3d). The different wetting properties in air and in ethanol also result in a *qualitatively* different response of $r$ to an increasing indentation depth $\delta$ and applied force $F$.

For an EGaIn droplet in air, in the limit of small loading force $|F| < 2$ nN, the right-hand side terms in eq 2 dominate and eq 2 simplifies to $\pi r^2(2\gamma/R) \approx 2\pi\gamma r \sin\theta$ and hence

$$r = R \sin\theta \tag{4}$$

That is, $r$ is relatively insensitive to $\delta$ and $F$ and only depends on the droplet radius $R$ and the contact angle $\theta$, which is a material property given by the Young's relation (eq 1).[42] As shown in Figure 3g, the numerical and experimental values of $r$ remain relatively constant on the approach curve: $r_{num}$ increases from 2.80 to 3.20 $\mu$m and $r_{exp}$ increases from 1.70 to 2.25 $\mu$m (an increase of between 15% and 30%), when increasing $\delta$ from 0 to 1 $\mu$m or equivalently $F$ from −1500 to 10 nN (position 1 to 2). We found that $r_{num}$ is systematically higher than $r_{exp}$, probably because our simplified analysis ignores the mechanical properties of the solid oxide layer, which exerts an additional repulsive force during the indentation process. We repeated the force spectroscopy measurements 18 times for droplets of different sizes $R$ = 3−15



https://doi.org/10.1021/acsnano.2c04667
ACS Nano 2022, 16, 14370−14378

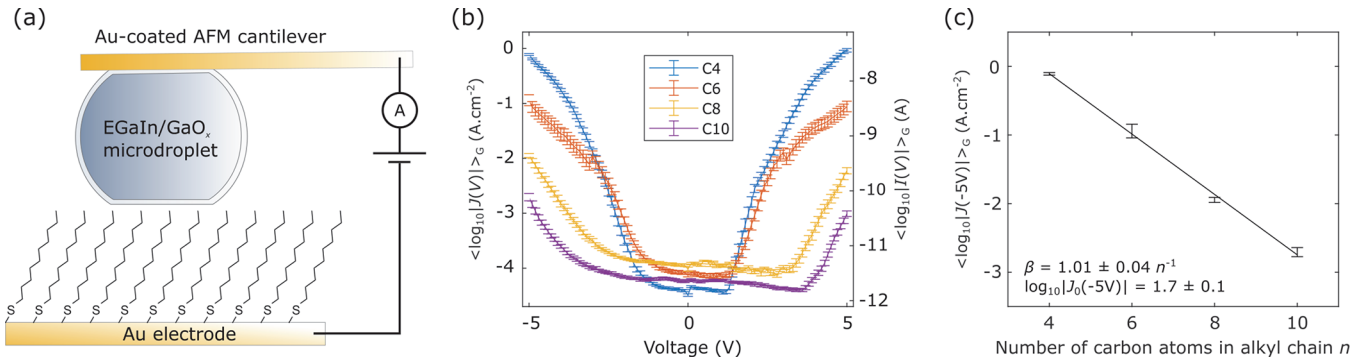


**Figure 4. (a) Schematic illustration of a molecular tunneling junction using EGaIn droplet probe AFM. (b) Plot of $\langle \log_{10}|J| \rangle_G$ and $\langle \log_{10}|I| \rangle_G$ ($|J|$ and $|I|$ in A cm$^{-2}$ and A, respectively) vs $V$ for junctions of different alkanethiol lengths C$n$. The EGaIn droplet has a diameter of 5 $\mu$m and contact diameter of 2 $\mu$m. (c) Plot of $\langle \log_{10}|J(-5V)| \rangle_G$ ($|J|$ in A cm$^{-2}$, voltage $V$ fixed at −5 V) vs $n$. For each alkanethiol, the results are averaged over at least 10 junctions with 40 sweeps per junction, and the error bars represent the 95% confidence interval from a Gaussian logarithmic fit to this data (detail of the statistical analysis in Supporting Figure S12 and Supporting Table S2).**

$\mu$m and found that $r_{exp}/R = 0.46 \pm 0.09$ or equivalently $\theta_{exp} = 152 \pm 6°$ (eq 4) for different alkanethiol surfaces and maximum applied force $F_{N,max} = 5-50$ nN (see Supporting Table S1), where the error is the standard error from the 18 measurements. We did not observe significant differences between alkanethiols of different lengths.

In contrast, for a highly nonwetting EGaIn droplet in ethanol, we expect

$$r = \sqrt{2R\delta} \tag{5}$$

in the limit of small $F$ and indentation depth $\delta = |z| \ll R$ (gray dashed-dot line in Figure 3h), which is in good agreement with the simulation results (solid blue line in Figure 3h). See Supporting Figure S7 for derivation of eq 5. In ethanol, $r$ increases more rapidly (in terms of percentage increase when compared to the same droplet in air) when increasing $\delta$ from 0 to 0.3 $\mu$m or equivalently $F$ from 0 to 45 nN, with $r_{num}$ increasing from 0.15 to 1.65 $\mu$m and $r_{exp}$ increasing from 0.55 to 1.15 $\mu$m (an increase of between 2 and 10 times). We cannot resolve $r_{exp} < 0.5$ $\mu$m because of the diffraction limit of the microscope. Therefore, we likely overestimate $r_{exp}$ values for small $\delta < 0.1$ $\mu$m, which partly explains the discrepancy between $r_{exp}$ and $r_{num}$.

A hysteresis-free force curve for highly nonwetting droplets (in ethanol) means more reproducible control of $r$, since $r$ only depends on the magnitude of applied force $F$ (and hence $\delta$) and not on how $F$ is applied, i.e., path and rate independent. This lack of hysteresis explains the symmetry between the approach and retract curves, i.e., about $z = 0.3$ $\mu$m for $r_{exp}$ and $r_{num}$ in Figure 3h. In contrast, $r$ in air depends not only on the magnitude of the applied force, but also on whether the droplet is approaching or retracting from the surface. This accounts for the asymmetry between the approach and retract curves, i.e., about $z = -1$ $\mu$m for $r_{exp}$ and $r_{num}$ in Figure 3g. We have repeated the force spectroscopy measurements for two additional droplets and found similar results as Figure 3 (see Supporting Figures S8 and S9).

Because of the small applied forces (<50 nN), the shape of the droplet can be described by the Young−Laplace equation, which is not the case for highly deformed EGaIn cone-shaped tips.[53] In our experiments, the oxide layer also remains intact even after multiple force spectroscopy measurements. For a spherical droplet of radius $R = 5$ $\mu$m with a contact radius $r = 1$ $\mu$m (corresponding to the maximum loading conditions of Figure 3h), we estimate the strain experienced by the oxide layer to be $\epsilon \approx 1/32(r/R)^4 \approx 2 \times 10^{-3}$ or 0.2%, below the reported yield strain of about 1%[50] (see derivation in Supporting Figure S7). The presence of an intact oxide is reflected in the absence of roughness/wrinkles in the SEM image and AFM topography map of the droplet in Figure 1 and Supporting Figure S1, both taken after performing several force spectroscopy measurements on the EGaIn droplet, indicating the robustness of the droplet probe tips. In contrast, the oxide layer can rupture when applying much larger loading forces (on the order of 100 $\mu$N), resulting in concentric cracks on the droplet (see Supporting Figure S10).[23] The presence of an intact oxide layer in our EGaIn microdroplets allows us to form stable molecular junctions, which we will describe in the next section.

**Micron-Sized Tunneling Junctions on SAMs.** We demonstrate an application of our proposed AFM technique by creating micrometer-sized molecular junctions.[33,54,55] Using droplet probes with radius $R = 1.5-2.5$ $\mu$m, we contacted the SAM surface in air with a maximum applied force of $F_{max} = 10$ nN and the resulting geometric contact radius $r = 0.5-1.2$ $\mu$m, similar in size to the typical grain size in template-stripped gold.[41] We then recorded the current $I$ as the voltage $V$ was varied in the range [−5 V, 5 V] using a source measure unit (Figure 4a). The current density $J$ can be obtained by dividing $I$ by the geometric contact area $a = \pi r^2$.

For each SAM (C4, C6, C8, and C10), we measured statistically large numbers of $J(V)$ curves (sample size $N = 383-600$ for each $n$) and constructed a Gaussian logarithmic average of $J$ values, $\langle \log_{10}|J| \rangle_G$ (where $J$ is in A cm$^{-2}$), versus $V$ curves following previously reported methods.[56,57] We observed a nonlinear increase of $\langle \log_{10}|J| \rangle_G$ with $V$ typical for coherent tunneling (Figure 4b), but the shape of $J(V)$ curves for $n = 4$ and 6 are concave and convex for $n = 8$ and 10, which could be caused by overbarrier (or Fowler Nordheim) tunneling.[58] Unfortunately, the currents at low voltage ($|V| \leq 2$ V) fall below the experimental noise, resulting in artifacts such as flat regions due to very low currents < 1 pA, preventing us from performing more detailed analysis.

For tunneling junctions, we expect $J = J_0 \exp(-\beta n)$, where $J_0$ is a pre-exponential factor that is often associated with the contact resistance, $\beta$ is the decay parameter, and $n$ is the number of carbon atoms in the molecule.[59−62] Experimentally,


https://doi.org/10.1021/acsnano.2c04667
ACS Nano 2022, 16, 14370−14378

we found that $\langle \log_{10}|J(-5V)|\rangle_G$ exhibits an exponential decay with increasing molecular length (Figure 4c), with the experimentally determined $\beta = 1.01 \pm 0.04\ n^{-1}$ consistent with previously reported values for tunnel junctions with *n*-alkanethiolate SAMs.[33−35] Despite having a smooth EGaIn droplet, the value of the pre-expontential factor $\log_{10}|J_0| = 1.7 \pm 0.1$ (where $|J_0|$ is in A cm$^{-2}$) measured at $V = -5$ V and with geometric contact areas $a = 4-12\ \mu m^2$ is lower than the reported values of $\log_{10}|J_0| = 2.2 \pm 0.3$ for EGaIn junctions based on cone-shaped tips measured at $V = 0.5$ V and with $a = 300-500\ \mu m^2$.[14,32,63] A possible explanation for this discrepancy is that the contact forces applied in the cone-shaped tip junctions (~$\mu$N)[24] are higher than in this work (~nN), resulting in plastic deformation of the oxide monolayer, a smaller tunneling gap, and hence higher $J_0$.[64] In this work, we also fabricated the microdroplets in ethanol (dispersant medium during ultrasonication) as opposed to air in cone-shaped tips, which can result in an oxide layer of different thickness and electrical conductivity. When exposed to ethanol, the EGaIn surface may become covered with a different adventitious layer than freshly prepared cone-shaped tips made in air.[1,65] Note that the rectification is expected to be negligible in Au/C*n*/EGaIn junctions; that is, the voltage polarity at which $J_0$ is extracted is not expected to lead to a significant difference.[32]

The junctions also show extreme robustness and can be subjected to voltages of up to 5 V, corresponding to an electrostatic stress of approximately 50 MV cm$^{-1}$, compared to a typical breakdown stress of ~8 MV cm$^{-1}$ in junctions formed using the EGaIn cone-shaped tip method.[36] This 5−6-fold increase in the breakdown field can likely be explained by the formation of smooth contact areas (with no wrinkles or cracks on the gallium oxide layer), which results in a homogeneous electrical field and current flow across the junctions. With rough contacts typically achieved with previous techniques, there can be "hot-spots" where the electrical field is locally high and breakdown can occur.[31,32] Additional experiments described in Supporting Figure S11 confirmed that most of the voltage drops across the SAM. Moreover, there are more intrinsic defects where breakdown can occur over the larger area of the cone as compared to EGaIn microspheres. The breakdown event in such structures has been attributed to the transfer of momentum from electrons to the metal atoms as the current passes through the structure, thus creating a conductive path and hence an electrical short circuit; this momentum transfer is referred to as the wind force.[36] As there is much lower current density *J* flowing through our EGaIn droplet probe system (and hence smaller wind force), we avoid such electrical breakdown in our structures.

The distributions in $\log_{10} J$ obtained with our droplet probe AFM measurements and more specifically its Gaussian standard deviation $\sigma_{\log,G} = 0.2-1.0$ (see Supporting Figure S12 and Table S2) are very similar to those obtained from junctions generated with cone-shaped tips, $\sigma_{\log,G} = 0.2-0.9$[31,41,56] indicating that the top electrode is not the limiting factor. Instead, defects in the bottom electrodes (such as grain boundaries, vacancy islands, or step edges) cause disorder in the SAMs and variations in *J*. This suggests that to improve the molecular junctions, we need to further optimize the substrate morphology (e.g., by using single-crystal electrode) and SAM's structural quality. Once optimized, our method can potentially be greatly beneficial for molecular electronics studies since in principle it is possible to contact the SAM on a single grain with micron-sized droplet probes.[31]

We chose not to perform any electrical measurements in ethanol because ethanol can become slightly conductive in the presence of contaminants, resulting in large background current.[66]

## CONCLUSIONS

We demonstrate a method to fabricate smooth EGaIn microdroplet probes and manipulate the droplets using an AFM to tune the droplet's contact area at the micron scale. We also explain how a highly nonwetting droplet is key to obtain reproducible, hysteresis-free contact. We form smooth, repeatable electrical contacts and molecular junctions of extreme stability, which allows us to address molecules over a larger voltage range previously inaccessible with other methods. Our technique and insight on EGaIn contact mechanics have relevance in many other applications such as nanowelding, plasmonics, and nanoelectronics, where precise positional control of liquid metal structures (including tuning EGaIn−substrate contact) is required.

## MATERIALS AND METHODS

**Tip Preparation.** To prepare EGaIn microspheres, 0.18 g of EGaIn (obtained from Alfa Aesar) is sonicated in 0.75 mL of ethanol for 30 min forming a grayish emulsion.[67] Subsequently, 10 $\mu$L of the emulsion is pipetted and drop-casted on the SAM substrate to be studied. Once the ethanol (VWR Chemicals) has evaporated away, we approach a suitably sized droplet with a tipless cantilever (MikroMasch HQ:NSC36, $k = 0.5-5$ N/m) with a set point force of 5 nN. We found that slight shearing while in contact with the droplet helps to release the droplet from the substrate, which can then be picked up easily. For tunneling experiments on SAMs, we replace the droplet after performing electrical characterizations after every 3−5 junctions. The attached droplet can be removed by rastering the cantilever on the surface in contact mode with a large applied force of more than 50 nN. A new droplet can then be selected and picked up to characterize the next junction.

**Template-Stripped Gold Surface Preparation.** We used the very well-known template-stripping method to fabricate ultrasmooth gold surfaces.[68] A Au film (purity of 99.99%, purchased from ACI Alloy, USA) of 15 nm is first thermally evaporated (DZ270, SKY Technology Development Co., Ltd., Shenyang, China, and Kurt J. Lesker Nano 36 Thermal Evaporator, Jefferson Hills, PA, USA) onto a prime-grade Si(100) wafer (SYST Integration Pte Ltd., Singapore). A 2 cm × 2 cm glass substrate was then glued to the Au layer using a Norland adhesive (Norland 61) which cures after 1 h under UV light. The glass substrate with the glued Au layer is then lifted off the Si wafer using a blade (template stripping). We have previously shown that the Au surfaces are ultraflat with a typical area grain size of $A_{gr} = 8 \times 10^5$ nm$^2$ and an rms roughness of less than 1 nm.[41] After template stripping, the gold surface is immediately used for SAM preparation to prevent contamination from the environment.

**Self-Assembly Monolayer Preparation.** The self-assembly process to obtain the alkanethiolate SAMs on Au was carried out similarly to previously reported methods.[62] Solutions of the alkanethiols were prepared in ethanol with a concentration of ~1 mM in an $N_2$ atmosphere. Au substrates were immersed and left overnight (~15 h) in the solutions in an $N_2$ atmosphere, collected the next day, rinsed with ethanol, and dried in a stream of $N_2$.

**Electrical Characterization of SAMs.** After picking up an EGaIn droplet, electrical contact is made by approaching the probe onto the SAM surface with a low applied force, typically 5−10 nN. We estimated the geometric contact area of the junction *a* by first measuring the droplet radius *R* with an optical microscope and applying eq 4, i.e., $a = \pi R^2 \sin^2\theta \approx 0.69R^2$, and using the average value of $\theta = 152°$ as reported in Supporting Table S1. The current


https://doi.org/10.1021/acsnano.2c04667
ACS Nano 2022, 16, 14370−14378

density $J$ can then be calculated by dividing $I$ by $a$. We did not directly measure $a$ under the microscope, because $a$ is smaller than the diffraction limit of the microscope for some of the droplets.

The voltage is swept in both directions in the range of between −5 and +5 V using a Keithley 4200-SCS source measure unit. A compliance of 0.1−1 μA is set to limit the current, preventing damage to both the probe and the SAM. For each molecular length of alkanethiol, at least 10 junctions were formed (on different locations) with 40 sweeps per junction with a current compliance applied, giving a total sample size of $N$ = 383−600 for the $I$−$V$ or $J$−$V$ curves. For each alkanethiol, 3−5 different droplets were used to check for consistency between droplets. See Supporting Figures S12 and S13 and Supporting Table S2 for details of the statistical analysis.

## ASSOCIATED CONTENT

### Supporting Information

The Supporting Information is available free of charge at https://pubs.acs.org/doi/10.1021/acsnano.2c04667.

Simulation of droplet contact in air (MOV)
Optical micrographs of droplet contact in air (MOV)
Simulation of droplet contact in ethanol (MOV)
Optical micrographs of droplet contact in ethanol (MOV)
Further details on the analysis of droplet geometry, the effect of droplet oxide for conductive measurements, droplet stability, statistical analysis, and the electrical measurement protocol (PDF)

## AUTHOR INFORMATION


### Corresponding Authors

**Dan Daniel** − *Institute of Materials Research and Engineering, Agency for Science, Technology and Research (A*STAR), Singapore 138634; Division of Physical Sciences and Engineering, King Abdullah University of Science and Technology (KAUST), Thuwal 23955-6900, Saudi Arabia;* orcid.org/0000-0002-5859-170X; Email: daniel@imre.a-star.edu.sg

**Sean J. O'Shea** − *Institute of Materials Research and Engineering, Agency for Science, Technology and Research (A*STAR), Singapore 138634;* orcid.org/0000-0003-0385-6245; Email: s-oshea@imre.a-star.edu.sg

**Harish Bhaskaran** − *Department of Materials, University of Oxford, Oxford OX1 3PH, United Kingdom;* orcid.org/0000-0003-0774-8110; Email: harish.bhaskaran@materials.ox.ac.uk

**Nikodem Tomczak** − *Institute of Materials Research and Engineering, Agency for Science, Technology and Research (A*STAR), Singapore 138634;* Email: tomczakn@imre.a-star.edu.sg

**Christian A. Nijhuis** − *Department of Chemistry, National University of Singapore, Singapore 117543; Hybrid Materials for Optoelectronics Group, Department of Molecules and Materials, MESA+ Institute for Nanotechnology and Center for Brain-Inspired Nano Systems, Faculty of Science and Technology, University of Twente, 7500 AE Enschede, The Netherlands;* orcid.org/0000-0003-3435-4600; Email: christian.nijhuis@nus.edu.sg

### Authors

**Eugene Jia Hao Soh** − *Department of Materials, University of Oxford, Oxford OX1 3PH, United Kingdom; Institute of Materials Research and Engineering, Agency for Science, Technology and Research (A*STAR), Singapore 138634;* orcid.org/0000-0001-6338-1320

**Hippolyte P. A. G. Astier** − *Department of Chemistry, National University of Singapore, Singapore 117543*

**Jia Qing Isaiah Chua** − *Biological and Biomimetic Material Laboratory, Center for Biomimetic Sensor Science, School of Materials Science and Engineering, Nanyang Technological University (NTU), Singapore 637553*

**Ali Miserez** − *Biological and Biomimetic Material Laboratory, Center for Biomimetic Sensor Science, School of Materials Science and Engineering, Nanyang Technological University (NTU), Singapore 637553;* orcid.org/0000-0003-0864-8170

**Zian Jia** − *Department of Mechanical Engineering, Virginia Polytechnic Institute and State University, Blacksburg, Virginia 24061, United States*

**Ling Li** − *Department of Mechanical Engineering, Virginia Polytechnic Institute and State University, Blacksburg, Virginia 24061, United States;* orcid.org/0000-0002-6741-9741

Complete contact information is available at: https://pubs.acs.org/10.1021/acsnano.2c04667


### Author Contributions

E.J.H.S., H.P.A.G.A., and D.D. contributed equally.

### Notes

The authors declare no competing financial interest.

## ACKNOWLEDGMENTS

D.D. acknowledges funding from A*STAR Competitive Research Fund (project number SC25/21-110411). N.T. is grateful to the Agency for Science, Technology and Research (A*STAR) for providing financial support under the Pharos Advanced Surfaces Programme (grant number 1523700101, project number SC25/16-2P1203).

## REFERENCES


(1) Lin, Y.; Cooper, C.; Wang, M.; Adams, J. J.; Genzer, J.; Dickey, M. D. Handwritten, soft circuit boards and antennas using liquid metal nanoparticles. *Small* **2015**, *11*, 6397−6403.

(2) Markvicka, E. J.; Bartlett, M. D.; Huang, X.; Majidi, C. An autonomously electrically self-healing liquid metal−elastomer composite for robust soft-matter robotics and electronics. *Nat. Mater.* **2018**, *17*, 618−624.

(3) Wang, M.; Trlica, C.; Khan, M. R.; Dickey, M. D.; Adams, J. J. A reconfigurable liquid metal antenna driven by electrochemically controlled capillarity. *J. Appl. Phys.* **2015**, *117*, 194901.

(4) Taccardi, N.; Grabau, M.; Debuschewitz, J.; Distaso, M.; Brandl, M.; Hock, R.; Maier, F.; Papp, C.; Erhard, J.; Neiss, C.; Peukert, W.; Gorling, A.; Steinruck, H.; Wasserscheid, P. Gallium-rich Pd−Ga phases as supported liquid metal catalysts. *Nat. Chem.* **2017**, *9*, 862−867.

(5) Park, S.; Thangavel, G.; Parida, K.; Li, S.; Lee, P. S. A stretchable and self-healing energy storage device based on mechanically and electrically restorative liquid-metal particles and carboxylated polyurethane composites. *Adv. Mater.* **2019**, *31*, 1805536.

(6) Guo, X.; Zhang, L.; Ding, Y.; Goodenough, J. B.; Yu, G. Room-temperature liquid metal and alloy systems for energy storage applications. *Energy Environ. Sci.* **2019**, *12*, 2605−2619.

(7) Wang, J.; Liu, S.; Vardeny, Z. V.; Nahata, A. Liquid metal-based plasmonics. *Opt. Express* **2012**, *20*, 2346−2353.

(8) Reineck, P.; Lin, Y.; Gibson, B. C.; Dickey, M. D.; Greentree, A. D.; Maksymov, I. S. UV plasmonic properties of colloidal liquid-metal eutectic gallium-indium alloy nanoparticles. *Sci. Rep.* **2019**, *9*, 1−7.

(9) Mayyas, M.; et al. Liquid-Metal-Templated Synthesis of 2D Graphitic Materials at Room Temperature. *Adv. Mater.* **2020**, *32*, 2001997.

(10) Chiechi, R. C.; Weiss, E. A.; Dickey, M. D.; Whitesides, G. M. Eutectic gallium−indium (EGaIn): a moldable liquid metal for electrical characterization of self-assembled monolayers. *Angew. Chem., Int. Ed.* **2008**, *47*, 142−144.
(11) Dickey, M. D.; Chiechi, R. C.; Larsen, R. J.; Weiss, E. A.; Weitz, D. A.; Whitesides, G. M. Eutectic gallium-indium (EGaIn): a liquid metal alloy for the formation of stable structures in microchannels at room temperature. *Adv. Funct. Mater.* **2008**, *18*, 1097−1104.
(12) Liu, Y.; Qiu, X.; Soni, S.; Chiechi, R. C. Charge transport through molecular ensembles: Recent progress in molecular electronics. *Chem. Phys.* **2021**, *2*, 021303.
(13) Thompson, D.; Nijhuis, C. A. Even the odd numbers help: failure modes of SAM-based tunnel junctions probed via odd-even effects revealed in synchrotrons and supercomputers. *Acc. Chem. Res.* **2016**, *49*, 2061−2069.
(14) Tostmann, H.; DiMasi, E.; Ocko, B. M.; Deutsch, M.; Pershan, P. S. X-ray studies of liquid metal surfaces. *J. Non. Cryst. Solids* **1999**, *250*, 182−190.
(15) Farrell, Z. J.; Tabor, C. Control of gallium oxide growth on liquid metal eutectic gallium/indium nanoparticles via thiolation. *Langmuir* **2018**, *34*, 234−240.
(16) Tevis, I. D.; Newcomb, L. B.; Thuo, M. Synthesis of liquid core−shell particles and solid patchy multicomponent particles by shearing liquids into complex particles (SLICE). *Langmuir* **2014**, *30*, 14308−14313.
(17) Yan, J.; Zhang, X.; Liu, Y.; Ye, Y.; Yu, J.; Chen, Q.; Wang, J.; Zhang, Y.; Hu, Q.; Kang, Y.; Yang, M.; Gu, Z. Shape-controlled synthesis of liquid metal nanodroplets for photothermal therapy. *Nano Res.* **2019**, *12*, 1313−1320.
(18) Xiong, M.; Gao, Y.; Liu, J. Fabrication of magnetic nano liquid metal fluid through loading of Ni nanoparticles into gallium or its alloy. *J. Magn. Magn. Mater.* **2014**, *354*, 279−283.
(19) Shu, J.; Tang, S.-Y.; Feng, Z.; Li, W.; Li, X.; Zhang, S. Unconventional locomotion of liquid metal droplets driven by magnetic fields. *Soft Matter* **2018**, *14*, 7113−7118.
(20) Ma, B.; Xu, C.; Chi, J.; Chen, J.; Zhao, C.; Liu, H. A versatile approach for direct patterning of liquid metal using magnetic field. *Adv. Funct. Mater.* **2019**, *29*, 1901370.
(21) Cheng, S.; Wu, Z. Microfluidic electronics. *Lab Chip* **2012**, *12*, 2782−2791.
(22) Cumby, B. L.; Hayes, G. J.; Dickey, M. D.; Justice, R. S.; Tabor, C. E.; Heikenfeld, J. C. Reconfigurable liquid metal circuits by Laplace pressure shaping. *Appl. Phys.* **2012**, *101*, 174102.
(23) Yunusa, M.; Amador, G. J.; Drotlef, D.-M.; Sitti, M. Wrinkling instability and adhesion of a highly bendable gallium oxide nanofilm encapsulating a liquid-gallium droplet. *Nano Lett.* **2018**, *18*, 2498−2504.
(24) Rothemund, R.; Morris, C. B.; Suo, Z.; Whitesides, G. M. Influence of the Contact Area on the Current Density across Molecular Tunneling Junctions Measured with EGaIn Top-Electrodes. *Chem. Mater.* **2018**, *30*, 129−137.
(25) Doudrick, K.; Liu, S.; Mutunga, E. M.; Klein, K. L.; Damle, V.; Varanasi, K. K.; Rykaczewski, K. Different shades of oxide: From nanoscale wetting mechanisms to contact printing of gallium-based liquid metals. *Langmuir* **2014**, *30*, 6867−6877.
(26) Joshipura, I. D.; Persson, K. A.; Truong, V. K.; Oh, J.; Kong, M.; Vong, M. H.; Ni, C.; Alsafatwi, M.; Parekh, D. P.; Zhao, H.; Dickey, M. D. Are contact angle measurements useful for oxide-coated liquid metals? *Langmuir* **2021**, *37*, 10914.
(27) Kramer, R. K.; Boley, J. W.; Stone, H. A.; Weaver, J. C.; Wood, R. J. Effect of microtextured surface topography on the wetting behavior of eutectic gallium−indium alloys. *Langmuir* **2014**, *30*, 533−539.
(28) Han, Y.; Nickle, C.; Zhang, Z.; Astier, H. P. A. G.; Duffin, T. J.; Qi, D.; Wang, Z.; Del Barco, E.; Thompson, D.; Nijhuis, C. A. Electric-field-driven dual-functional molecular switches in tunnel junctions. *Nat. Mater.* **2020**, *19*, 843−848.
(29) Han, Y.; Nijhuis, C. A. Functional Redox-Active Molecular Tunnel Junctions. *Asian J. Chem.* **2020**, *15*, 3752−3770.
(30) Simeone, F. C.; Yoon, H. J.; Thuo, M. M.; Barber, J. R.; Smith, B.; Whitesides, G. M. Defining the value of injection current and effective electrical contact area for EGaIn-based molecular tunneling junctions. *J. Am. Chem. Soc.* **2013**, *135*, 18131−18144.
(31) Jiang, L.; Sangeeth, C. S. S.; Wan, A.; Vilan, A.; Nijhuis, C. A. Defect scaling with contact area in egain-based junctions: impact on quality, joule heating, and apparent injection current. *J. Phys. Chem. C* **2015**, *119*, 960−969.
(32) Chen, X.; Hu, H.; Trasobares, J.; Nijhuis, C. A. Rectification ratio and tunneling decay coefficient depend on the contact geometry revealed by in situ imaging of the formation of EGaIn junctions. *ACS Appl. Mater. Interfaces* **2019**, *11*, 21018−21029.
(33) Karuppannan, S. K.; Neoh, E. H. L.; Vilan, A.; Nijhuis, C. A. Protective Layers Based on Carbon Paint To Yield High-Quality Large-Area Molecular Junctions with Low Contact Resistance. *J. Am. Chem. Soc.* **2020**, *142*, 3513−3524.
(34) Vilan, A.; Aswal, D.; Cahen, D. Large-area, ensemble molecular electronics: motivation and challenges. *Chem. Rev.* **2017**, *117*, 4248−4286.
(35) Metzger, R. M. Unimolecular electronics. *Chem. Rev.* **2015**, *115*, 5056−5115.
(36) Yuan, L.; Jiang, L.; Nijhuis, C. A. The Drive Force of Electrical Breakdown of Large-Area Molecular Tunnel Junctions. *Adv. Funct. Mater.* **2018**, *28*, 1801710.
(37) Çınar, S.; Tevis, I. D.; Chen, J.; Thuo, M. Mechanical fracturing of core-shell undercooled metal particles for heat-free soldering. *Sci. Rep.* **2016**, *6*, 1−12.
(38) Chintala, R.; Eyben, P.; Armini, S.; Caro, A. M.; Loyo, J.; Sun, Y.; Vandervorst, W. Electrical properties of amino SAM layers studied with conductive AFM. *Eur. Polym. J.* **2013**, *49*, 1952−1956.
(39) Larsen, R. J.; Dickey, M. D.; Whitesides, G. M.; Weitz, D. A. Viscoelastic properties of oxide-coated liquid metals. *J. Rheol.* **2009**, *53*, 1305−1326.
(40) Shen, J.; Zhang, D.; Zhang, F.-H.; Gan, Y. AFM tip-sample convolution effects for cylinder protrusions. *Appl. Surf. Sci.* **2017**, *422*, 482−491.
(41) Yuan, L.; Jiang, L.; Zhang, B.; Nijhuis, C. A. Dependency of the tunneling decay coefficient in molecular tunneling junctions on the topography of the bottom electrodes. *Angew. Chem.* **2014**, *126*, 3445−3449.
(42) de Gennes, P.-G.; Brochard-Wyart, F.; Quéré, D. *Capillarity and Wetting Phenomena: Drops, Bubbles, Pearls, Waves*, 1st ed.; Springer: New York, NY, 2004; pp 1−78.
(43) Daniel, D.; Chia, A. Y. T.; Moh, L. C. H.; Liu, R.; Koh, X. Q.; Zhang, X.; Tomczak, N. Hydration Lubrication of Polyzwitterionic Brushes Leads to Nearly Friction- and Adhesion-Free Droplet Motion. *Comm. Phys.* **2019**, *2*, 105.
(44) Daniel, D.; Florida, Y.; Lay, C. L.; Koh, X. Q.; Sng, A.; Tomczak, N. Quantifying Surface Wetting Properties Using Droplet Probe Atomic Force Microscopy. *ACS Appl. Mater. Interfaces* **2020**, *12*, 42386−42392.
(45) Xie, L.; Shi, C.; Cui, X.; Zeng, H. Surface Forces and Interaction Mechanisms of Emulsion Drops and Gas Bubbles in Complex Fluids. *Langmuir* **2017**, *33*, 3911−3925.
(46) Escobar, J. V.; Garza, C.; Castillo, R. Measuring Adhesion on Rough Surfaces Using Atomic Force Microscopy with a liquid probe. *Beilstein J. Nanotechnol.* **2017**, *8*, 813−825.
(47) Harrison, A. J.; Corti, D. S.; Beaudoin, S. P. Capillary forces in nanoparticle adhesion: a review of AFM methods. *Part. Sci. Technol.* **2015**, *33*, 526−538.
(48) Berry, J. D.; Neeson, M. J.; Dagastine, R. R.; Chan, D. Y. C.; Tabor, R. F. Measurement of surface and interfacial tension using pendant drop tensiometry. *J. Colloid Interface Sci.* **2015**, *454*, 226−237.
(49) Handschuh-Wang, S.; Chen, Y.; Zhu, L.; Zhou, X. Analysis and Transformations of Room-Temperature Liquid Metal Interfaces−A Closer Look through Interfacial Tension. *Chem. Phys. Chem.* **2018**, *19*, 1584−1592.


https://doi.org/10.1021/acsnano.2c04667
*ACS Nano* 2022, 16, 14370−14378

(50) Jacob, A. R.; Parekh, D. P.; Dickey, M. D.; Hsiao, L. C. Interfacial rheology of gallium-based liquid metals. *Langmuir* **2019**, *35*, 11774−11783.
(51) Morris, N. J.; Farrell, Z. J.; Tabor, C. E. Chemically modifying the mechanical properties of core−shell liquid metal nanoparticles. *Nanoscale* **2019**, *11*, 17308−17318.
(52) Daniel, D.; Lay, C. L.; Sng, A.; Lee, C. J. J.; Neo, D. C. J.; Ling, X. Y.; Tomczak, N. Mapping Micrometer-Scale Wetting Properties of Superhydrophobic Surfaces. *Proc. Natl. Acad. Sci. U.S.A.* **2019**, *116*, 50.
(53) Knoche, S.; Vella, D.; Aumaitre, E.; Degen, P.; Rehage, H.; Cicuta, P.; Kierfeld, J. Elastometry of deflated capsules: Elastic moduli from shape and wrinkle analysis. *Langmuir* **2013**, *29*, 12463−12471.
(54) Puebla-Hellmann, G.; Venkatesan, K.; Mayor, M.; Lörtscher, E. Metallic nanoparticle contacts for high-yield, ambient-stable molecular-monolayer devices. *Nature* **2018**, *559*, 232−235.
(55) Jeong, H.; Kim, D.; Kim, P.; Cho, M. R.; Hwang, W.-T.; Jang, Y.; Cho, K.; Min, M.; Xiang, D.; Park, Y. D.; Jeong, H.; Lee, T. A new approach for high-yield metal-molecule-metal junctions by direct metal transfer method. *Nanotechnology* **2015**, *26*, 025601.
(56) Reus, W. F.; Nijhuis, C. A.; Barber, J. R.; Thuo, M. M.; Tricard, S.; Whitesides, G. M. Statistical tools for analyzing measurements of charge transport. *J. Phys. Chem. C* **2012**, *116*, 6714−6733.
(57) Gupta, N. K.; Wilkinson, E. A.; Karuppannan, S. K.; Bailey, L.; Vilan, A.; Zhang, Z.; Qi, D.-C.; Tadich, A.; Tuite, E. M.; Pike, A. R.; Tucker, J. H. R.; Nijhuis, C. A. Role of order in the mechanism of charge transport across single-stranded and double-stranded DNA monolayers in tunnel junctions. *J. Am. Chem. Soc.* **2021**, *143*, 20309−20319.
(58) Vilan, A. Analyzing molecular current-voltage characteristics with the Simmons tunneling model: scaling and linearization. *J. Phys. Chem. C* **2007**, *111*, 4431−4444.
(59) Xie, Z.; Bâldea, I.; Oram, S.; Smith, C. E.; Frisbie, C. D. Effect of heteroatom substitution on transport in alkanedithiol-based molecular tunnel junctions: evidence for universal behavior. *ACS Nano* **2017**, *11*, 569−578.
(60) Chen, X.; Nijhuis, C. A. The unusual dielectric response of large area molecular tunnel junctions probed with impedance spectroscopy. *Adv. Electron. Mater.* **2021**, 2100495.
(61) Jeong, H.; Kim, D.; Xiang, D.; Lee, T. High-yield functional molecular electronic devices. *ACS Nano* **2017**, *11*, 6511−6548.
(62) Jiang, L.; Sangeeth, C. S. S.; Nijhuis, C. A. The origin of the odd−even effect in the tunneling rates across EGaIn junctions with self-assembled monolayers (SAMs) of n-alkanethiolates. *J. Am. Chem. Soc.* **2015**, *137*, 10659−10667.
(63) Yuan, L.; Jiang, L.; Thompson, D.; Nijhuis, C. A. On the remarkable role of surface topography of the bottom electrodes in blocking leakage currents in molecular diodes. *J. Am. Chem. Soc.* **2014**, *136*, 6554−6557.
(64) Gosvami, N. N.; Sinha, S. K.; Srinivasan, M. P.; O'Shea, S. J. Effect of surrounding medium on resistance of a molecular monolayer junction. *J. Phys. Chem. C* **2008**, *112*, 297−302.
(65) Cademartiri, L.; Thuo, M. M.; Nijhuis, C. A.; Reus, W. F.; Tricard, S.; Barber, J. R.; Sodhi, R. N. S.; Brodersen, P.; Kim, C.; Chiechi, R. C.; Whitesides, G. M. Electrical resistance of AgTS−S$(CH_2)_{n-1}CH_3$//$Ga_2O_3$/EGaIn tunneling junctions. *J. Phys. Chem. C* **2012**, *116*, 10848−10860.
(66) Luecke, J.; McCormick, R. L. Electrical conductivity and pHe response of fuel ethanol contaminants. *Energy Fuels* **2014**, *28*, 5222−5228.
(67) Hohman, J. N.; Kim, M.; Wadsworth, G. A.; Bednar, H. R.; Jiang, J.; LeThai, M. A.; Weiss, P. S. Directing substrate morphology via self-assembly: ligand-mediated scission of gallium−indium microspheres to the nanoscale. *Nano Lett.* **2011**, *11*, 5104−5110.
(68) Vogel, N.; Zieleniecki, J.; Köper, I. As flat as it gets: ultrasmooth surfaces from template-stripping procedures. *Nanoscale* **2012**, *4*, 3820−3832.




https://doi.org/10.1021/acsnano.2c04667
*ACS Nano* 2022, 16, 14370−14378